

5-(3-Pyridyl)-4H-1,2,4-triazole-3-thiol as Potential Corrosion Inhibitor for AA6061 Aluminium Alloy in 0.1 M Hydrochloric Acid Solution

K. Raviprabha^a and Ramesh S. Bhat^{b, *}

^aDepartment of Chemistry, Shri Madhwa Vadiraja Institute of Technology and Management, Bantakal, Karnataka, UDUPI-574-115 India

^bDepartment of Chemistry, NMAM Institute of Technology, Karkala, Nitte-574110 India

*e-mail: rameshbhat@nitte.edu.in

Received January 31, 2019; revised February 13, 2019; accepted February 15, 2019

Abstract—Corrosion inhibition performance of 5-(3-Pyridyl)-4H-1,2,4-triazole-3-thiol on aluminium alloy AA6061 in 0.1 M HCl solution was tested by the weight loss method, potentiodynamic polarization and electrochemical impedance spectroscopy. The effect of an increase in temperature and a change in the concentration of the inhibitor were studied. The results indicated that with an increase in the concentration of the inhibitor and temperature the inhibition efficiency also increased. The inhibition efficiency as high as 94.1% was found at 60°C for 40 ppm of the inhibitor. By the perusal of thermodynamic and activation parameters, it is found that adsorption of the studied inhibitor takes place through chemisorption. The inhibitor agrees the Langmuir adsorption isotherm and acts as a mixed type inhibitor. Thermodynamic parameters also unveiled that the process of adsorption on the metal surface takes place through chemisorption. The formation of a protective film on the metal surface was confirmed by scanning electron microscopy. From the mechanism of corrosion inhibition, it is possible to deduce the formation of a coordination bond between the inhibitor and the metal surface. The inhibition nature of the molecule was explained by theoretical studies.

Keywords: aluminium alloy AA6061, corrosion inhibitor, electrochemical impedance spectroscopy, scanning electron spectroscopy

DOI: 10.3103/S1068375519060103

INTRODUCTION

Corrosion is a destructive (or deterioration) attack on metals and alloys by chemical or electrochemical reactions whenever it is exposed to a corrosive atmosphere. Aluminium is widely used in manufacturing automobiles, aircrafts, household appliances, containers, and electronic devices [1]. The structural components of aircrafts or submarines are largely fabricated from high strength Al alloys that contain alloying elements like Cu, Mg, Fe, Si and Mn [2, 3]. Such alloys have acceptable mechanical properties and higher strength to weight ratios. Aluminium and its alloys finds potential applications in the field of industries, building constructions, kitchen, defence, automobile and electronics etc., even with its higher susceptibility to corrosion due to its low reduction potential of -1.66 V and higher oxidation tendency [4, 5].

Aluminium shows resistance to corrosion due to the formation of a stable metal oxide film [6]. But in the presence of an acidic medium like hydrochloric acid, the amphoteric oxide film gets ruptured when the pH falls below 4. Acidic solutions are widely used in industries for surface cleaning techniques. These

are obligatory for almost all metal specimens, even for the most expensive coatings. Surface cleaning techniques include pre-finishing operations such as stripping, pickling, and chemical cleaning process [7, 8]. A corrosion problem takes place as a result of the interface between aqueous acidic solutions and the metals, especially during the pickling process in which an alloy is brought in contact with concentrated acids. This process if not combated can lead to economic losses due to the corrosion of the alloy [9].

The use of a corrosion inhibitor is one of the best methods for the protection of metals from corrosion. Most of the inhibitors used are organic compounds having heteroatoms, unsaturated bonds/aromatic rings which can donate lone pairs of electrons such as phosphorus, sulphur, nitrogen, and π electrons, through which inhibitor molecules interact with the metal surface by which adsorption takes place [10–12]. Most of the inhibitors are toxic, even though they exhibit superior inhibition properties. The anticorrosion properties of a novel compound 2-(4-(diethylamino)-2-hydroxybenzylidene) hydrazinecarboamide on the aluminium alloy AA2024-T3 in 0.5 M HCl

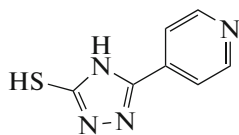


Fig. 1. Chemical structure of PHTT molecule.

solution at 303 K were studied by the electrochemical and weight loss methods and its inhibition efficiency was found to increase with an increase in concentration [13].

The AA6061 alloy is more susceptible for corrosion in acidic solutions. Hydrochloric acid is generally used for electrochemical etching of aluminium and its alloys. The dissolution of an aluminium alloy in HCl solution can be avoided by the addition of inhibitors to the acidic medium. Almost all organic inhibitors have the capacity to prevent the corrosion of metals by the formation of an insoluble self barrier or coating on the base metal surface. In general, organic inhibitors are adsorbed on the metal surface by chemisorptions through the formation of strong coordination bonds with the metal surface during electrostatic interface between the charged metal surface and inhibitors [14].

The current study explains the influence of 5-(3-Pyridyl)-4H-1,2,4-triazole-3-thiol (PHTT) as corrosion inhibitor for AA6061 in 0.1 M HCl solution. Alloy coupons were tested by the weight loss method, potentiodynamic polarisation (PDP) and electrochemical impedance spectroscopy (EIS). The mechanism of adsorption by the inhibitor was studied by considering the effect of temperature as well as activation and thermodynamic parameters.

EXPERIMENTAL

Preparation of Specimens

The aluminium alloy AA6061 specimens with the composition (wt.%) Si(0.6), Cu(0.25), Mg(1.0), Cr(0.25), and Al(balance) were used in the study. Each specimen was in the form of a cylindrical rod with 1.31 cm² open surface area, the remaining was entrenched in epoxy resin. According to the metallographic practice, the specimens were subjected to belt grinding and polishing using various grades of emery paper and mirror finished on disc polishing using legated alumina as abrasive. Then the specimens were cleaned with double distilled water followed by acetone, finally dried, and immediately used for the analysis.

Preparation of Medium

The acid solution (0.1 M HCl) was prepared by using an analytical grade reagent (Merck) of 37% HCl and double distilled water. The standardization of HCl was done with standard NaOH solution by volumetric method. From the standard solution, the required

concentration of HCl (0.1 M) solution was prepared as and when required. Experiments were carried out using calibrated thermostat at temperatures 30°, 40°, 50°, 60°C under unstirred and aerated conditions. The inhibitive effect was studied by using 10–40 ppm of PHTT into acid solutions. The molecular structure of PHTT is given in Figure 1.

Weight Loss Method

The AA6061 alloy coupons of dimensions 1.5 × 2.5 × 1 cm were used for weight loss measurements. The weight loss was determined at different immersion times: 25, 50, and 75 h at 30°C by weighing the specimens before and after immersing in 100 mL of 0.1 M HCl in a 250 ml open beaker with and without PHTT. After the immersion period, the specimens were removed from the medium, cleaned by wiping the coupons with tissue paper, washed with distilled water followed by acetone, dried and then weighed. The inhibition efficiency and the corrosion rate were calculated using Equations 1 and 2, respectively.

$$IE(\%) = \frac{W_{un} - W_{in}}{W_{un}} \times 100 ; \quad (1)$$

$$CR(\text{mm/year}) = 87.6 \times (W/DAT), \quad (2)$$

where A is the area of the specimen in cm²; T is the immersion time in hours; W_{un} and W_{in} are the weight loss values without and with inhibitors, respectively.

Electrochemical Studies

Electrochemical measurements of AA6061 were carried out by using a potentiostat CH604 E-series, with CH-instrument beta software. Both polarization studies and electrochemical impedance measurements (EIS) were carried out using a conventional three-electrode glass cell with a platinum counter electrode, a saturated calomel electrode as reference, and AA6061 specimen as working electrode. The freshly polished specimen was exposed to a corrosive medium of 0.1 M hydrochloric acid in the presence or the absence of PHTT at different temperatures and allowed to establish a steady state open circuit potential (OCP). PDP measurements were done by polarizing the specimen from –250 mV cathodically to +250 mV anodically, with respect to the OCP, at a scan rate of 1 mV s⁻¹; and the PDP plots were recorded. The experiments were performed at different temperatures using a calibrated thermostat. The corrosion potential and the corrosion current density were recorded, from which the corrosion rate and the percentage inhibition efficiency were calculated. The EIS studies were done by impressing 10 mV of a small amplitude AC signal on the OCP with a frequency range from 10000 Hz to 0.01 Hz. Nyquist plots were used for the analysis of the impedance data to assess corrosion characteristics. The charge transfer resistance and the double layer capacitance were deduced from the simulation of the

Table 1. Results of weight loss method with various concentrations of PHTT at 50°C

Immersion time (Hours)	Conc. of inhibitor	Wt. loss, mg	Corrosion rate, mm y ⁻¹	%IE
25	Blank	25.5	2.758	—
	10 ppm	6.3	0.681	75.3
	20 ppm	5.8	0.627	77.3
	30 ppm	5.0	0.541	80.4
	40 ppm	4.0	0.433	84.3
50	Blank	53.3	2.882	—
	10 ppm	10.8	0.584	79.7
	20 ppm	8.5	0.460	84.1
	30 ppm	6.5	0.351	87.8
	40 ppm	5.3	0.287	90.1
75	Blank	89.9	3.241	—
	10 ppm	12.5	0.451	86.1
	20 ppm	10.1	0.364	88.8
	30 ppm	8.2	0.296	90.9
	40 ppm	7.3	0.263	91.9

impedance data with an equivalent circuit fitment using ZSimpWin version 3.21 software.

Surface Morphology Studies

Surface morphology studies of AA6061 were carried out by using an analytical scanning electron microscope (JEOL JSM-6380L), in the magnification of 1000X. The surface morphology of the metal samples was obtained by immersing the specimens in hydrochloric acid medium for 2 h without and with 40 ppm of the inhibitor.

RESULTS AND DISCUSSION

Weight Loss Method

The variations of the weight loss of AA6061 in 0.1 M HCl with and without the addition of different concentrations of PHTT, at various immersion time periods, have been studied. The weight loss, the corrosion rate, and inhibition efficiencies are presented in Table 1. The inhibition efficiency improved in leaps and bounds with a fourfold increase in the concentration of the inhibitor from 75.3 to 91.9%. The variations in the weight loss and the inhibition efficiency of PHTT at varying immersion times are shown in Figs. 2 and 3. At 40 ppm, PHTT showed the maximum inhibition efficiency of 91.9%. Above that concentration, almost the same efficiency was obtained; therefore it is considered to be the optimum concentration for achieving the maximum inhibition efficiency.

Potentiodynamic Polarization Measurements

The effect of the inhibitor concentration on the corrosion rate of AA6061 was studied. Figure 4 presents the PDP plots for the corrosion of AA6061 in 0.1 M HCl solution at 50°C in the presence of varying concentrations of the inhibitor. The electrochemical parameters such as the corrosion current density (i_{corr}), the corrosion potential (E_{corr}), were obtained from the polarization studies. The corrosion rate (CR) in mm·y⁻¹ was obtained by using Equation (3):

$$CR = \frac{3270Mi_{\text{corr}}}{\rho Z}, \quad (3)$$

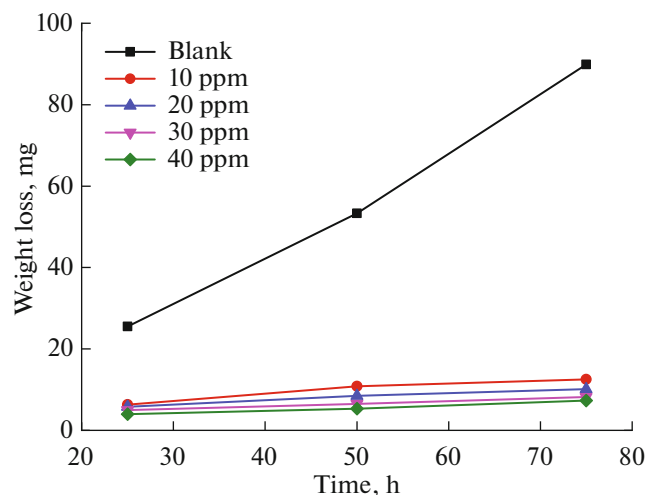


Fig. 2. Variations of weight loss against time for the corrosion inhibition of AA6061 at 50°C.

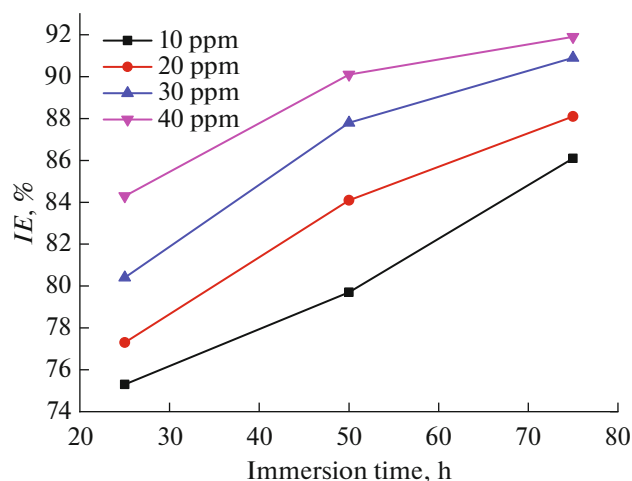


Fig. 3. Variations in inhibition efficiency of inhibitor in 0.1 M HCl against immersion time at various concentrations.

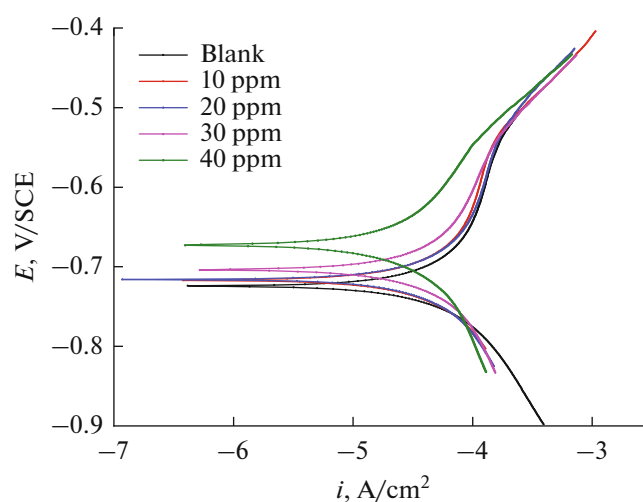


Fig. 4. PDP curves for corrosion of AA6061 in 0.1 M HCl containing varying concentrations of inhibitor at 50°C.

where 3270 is a constant that defines the unit of the corrosion rate, ρ is the density of the corroding material (2.7 g cm^{-3}), M is the atomic mass of the metal (27), Z is the number of electrons transferred per metal atom [15]. The percentage inhibition efficiency of the inhibitor may be calculated by using Equation (4):

$$\eta = \frac{i_{\text{corr(un)}} - i_{\text{corr(in)}}}{i_{\text{corr(un)}}} \times 100, \quad (4)$$

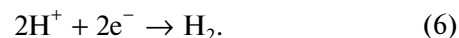
where $i_{\text{corr(un)}}$ and $i_{\text{corr(in)}}$ are the corrosion current densities in the absence or in the presence of the inhibitor, respectively. The results of PDP measurements for the corrosion of AA6061 in 0.1 M HCl containing various concentrations of the inhibitor at different temperatures are in Table 2. It is evident that the corrosion current density and the corrosion rate values decrease in the presence of different concentrations of the inhibitor. Hence, the inhibition efficiency increases with an increase in the inhibitor concentration. At a higher temperature, e.g., at 60°C, the highest corrosion rate has been found in the blank sample, while the inhibition efficiency was the highest (94.2%) at 60°C. This is mainly because of adsorption of the inhibitor on the Al surface. The adsorbed inhibitor molecules create a protective self barrier between the Al surface and the aggressive medium [16].

It is reported in literature [17–19] that, if the corrosion potential value of the inhibited solution is less than $\pm 85 \text{ mV}$ with respect to the uninhibited solution, then the inhibitor can be considered distinctively as anodic and cathodic inhibitor. However, in the present study, the maximum displacement was much lower than $\pm 85 \text{ mV}$. This suggests that PHTT may act as a mixed type inhibitor, with predominance of anodic inhibition. The shapes of polarization curves in the absence or the presence of the inhibitor (Fig. 4) are similar, which suggested that the hydrogen evolution is activated-controlled and it does not alter the mecha-

nism of the reduction reaction [20, 21]. The slopes of both anodic (β_a) and cathodic (β_c) Tafel lines did not vary significantly with an increase in the inhibitor concentration, which indicates that the hydrogen evolution is activation-controlled and the presence of the inhibitor does not change the mechanism of inhibition. The added inhibitor stops the anodic reaction and supports for the passivation of an oxide film on the metal surface and also the inhibitor impairs the anodic oxidation process:



and also impedes cathodic hydrogen liberation reaction [22]:



This proves that the studied organic inhibitor functions as mixed type inhibitor.

Electrochemical Impedance Spectroscopy Measurements

The Nyquist plots for the corrosion inhibition of AA6061 in 0.1 M HCl medium at various concentration of PHTT at 50°C as shown in Fig. 5. The data obtained from EIS studies give the information on the type of an electrochemical process occurred at the electrode/electrolyte interface. The Nyquist plots are deviated semicircles due to the frequency dispersion of interfacial impedance, attributable to the roughness and non-homogeneity of the electrode surface and to the adsorption of the inhibitor and formation of porous layers [23]. The impedance spectra showed a semicircle, which indicates that corrosion is mainly controlled by the charge transfer process. In this Figure, the high frequency region corresponds to a large capacitive loop while the low frequency region indicates a small inductive loop. The large capacitive loop represents the charge transfer during corrosion process

Table 2. Results of PDP measurements for corrosion of AA6061 in 0.1 M HCl at various concentrations of inhibitor

Temp, °C	Conc. of inhibitor, ppm	β_a , mV dec ⁻¹	β_b , mV dec ⁻¹	$-E_{\text{corr}}$, V/SCE	I_{corr} , mA cm ⁻²	CR, mm y ⁻¹	%IE
30	Blank	658	345	727.8	1.894	11.7	–
	10	715	404	715.1	0.359	2.23	81.0
	20	685	357	710.5	0.301	1.87	84.1
	30	729	405	705.4	0.271	1.68	85.6
	40	638	335	702.2	0.241	1.49	87.2
40	Blank	426	381	718.5	3.352	20.8	–
	10	466	371	715.9	0.413	2.56	87.4
	20	483	360	705.3	0.338	2.10	89.7
	30	457	350	701.6	0.275	1.66	91.6
	40	427	343	690.3	0.246	1.53	92.5
50	Blank	371	508	730.5	6.458	40.0	–
	10	386	544	707.8	0.696	4.32	88.1
	20	362	448	695.6	0.506	3.14	91.3
	30	339	438	690.9	0.428	2.65	92.6
	40	481	563	685.4	0.377	2.34	93.4
60	Blank	359	516	743.2	12.43	77.0	–
	10	376	520	680.1	1.301	8.07	88.5
	20	405	546	676.8	0.843	5.23	92.5
	30	425	535	668.8	0.694	4.30	93.8
	40	468	566	652.4	0.648	4.02	94.2

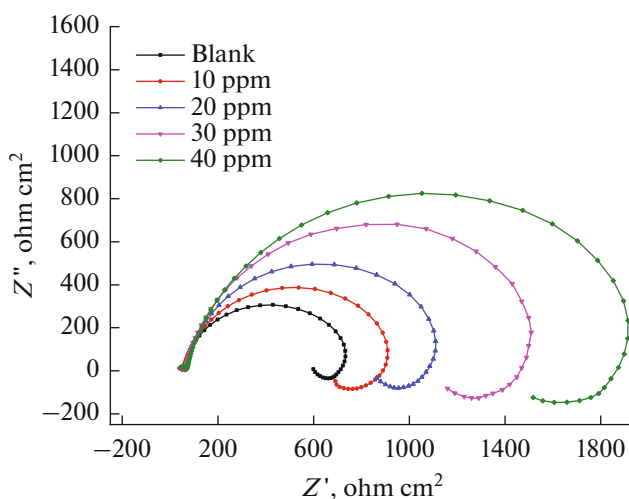
and development of an oxide layer on the metal surface [24]. The origin of the inductive loop has been attributed to the surface or bulk relaxation of species in the oxide layer [25]. That loop may be related to the relaxation process obtained by adsorption and incorporation of chloride ions, oxide ions, or charged species on the electrode surface [26]. The Nyquist plot obtained for the corrosion control of AA6061 shows that the diameter of the capacitive loop increased with an increase in the inhibitor concentration, which is due to a decrease of the corrosion rate by the adsorption of the inhibitor molecule onto the surface of the metal.

The impedance parameters were analysed by fitting a suitable equivalent circuit to the Nyquist plots using ZSimpWin software version 3.21. Figure 6 shows the equivalent circuit which was used to simulate the impedance plot for AA6061. The equivalent circuit consists of nine elements. They are: the solution resistance (R_s) and the charge transfer resistance (R_{ct}), the inductive resistance (R_L) and the inductive element (L). The constant phase element (CPE) Q is parallel to the series of capacitors C_1 and C_2 and parallel to the series of resistor R_1 , R_2 , R_L , and R_{ct} . R_L is parallel to L inductor. The parallel circuit of a resistor is attributed for an oxide film due to the ionic conduction in the oxide film and the capacitance due to its dielectric properties. The double layer capacitance (C_{dl}) and

polarization resistance (R_p) can be calculated by using Equations 7 and 8, respectively:

$$R_p = R_1 + R_2 + R_L + R_{ct}; \quad (7)$$

$$C_{dl} = C_1 + C_2. \quad (8)$$

**Fig. 5.** Nyquist plots for corrosion inhibition of AA6061 in 0.1 M HCl at various concentrations of inhibitor at 50°C.

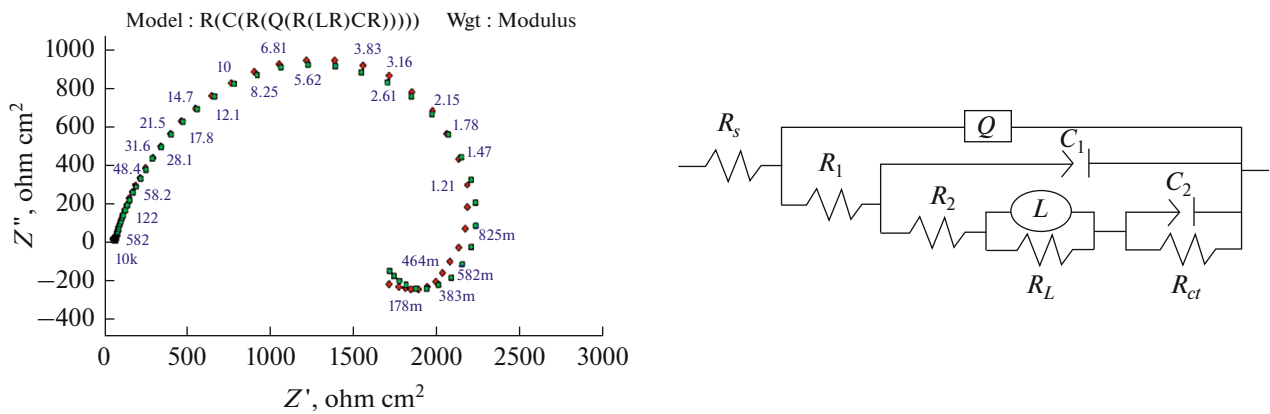


Fig. 6. a. Simulated plot obtained from the circuit fitment. b. Equivalent circuit used to simulate the impedance plot for AA6061 in 0.1 M HCl at 40 ppm of inhibitor concentrations at 50°C.

The EIS parameters obtained are reported in Table 3. The CPE impedance was calculated using Equation 9, borrowed from [27]:

$$Z = A^{-1} (i\omega)^{-n}, \quad (9)$$

where A is the proportionality constant, ω is the angular frequency, i is the imaginary number, and n is the exponent related to the phase shift. If the value of $n = 1$, then the CPE behaves like an ideal capacitor. The correlation in the capacitance to its real value was calculated using Equation 10, borrowed from [28]:

$$C_{dl} = \frac{1}{2\pi f_{\max} R_{ct}}, \quad (10)$$

where f_{\max} is the frequency at which the imaginary component of impedance is maximum and R_{ct} is the charge transfer resistance. According to Table 3, the measured C_{dl} value decreased with an increase in concentrations of the inhibitor at all temperatures; it resulted from an increase in the electrical double layer at the metal solution interface. A further decrease in the C_{dl} values was caused by a gradual replacement of water molecules by inhibitor molecules. The polarization resistance (R_p) values varied inversely with the corrosion current density (i_{corr}). The inhibition efficiency was obtained using Equation 11:

$$IE\% = \frac{R_{p(\text{inh})} - R_p}{R_{p(\text{inh})}} \times 100, \quad (11)$$

where R_p and $R_{p(\text{inh})}$ are the polarization resistances in the absence or in the presence of the inhibitor, respectively. R_p values increased with an increase in the concentration of the inhibitor. This results in lowering the value of double layer capacitance (C_{dl}), indicates that the charge transfer process is mainly controlling the corrosion process.

Effect of Temperature

The effect of temperature on the corrosion rate of AA6061 in 0.1 M HCl and on the inhibition efficiency of PHTT was studied at temperatures in a range of 30–60°C, from which the kinetic and thermodynamic parameters for the corrosion inhibition were calculated. The corrosion activation energy in the presence or in the absence of the inhibitor and the dependence of the inhibitor adsorption on temperature can be interpreted via the adsorption mechanism. The Tafel polarisation curves and the Nyquists plots for AA6061 at different temperatures in 0.1 M HCl solution are shown in Figs. 7 and 8. The energy of activation is calculated using Arrhenius equation 12, borrowed from [29]:

$$\ln(CR) = A - \frac{E_a}{RT}, \quad (12)$$

where E_a is the activation energy, A is the Arrhenius pre-exponential constant, R is the universal gas constant and T is absolute temperature. The plot of $\ln(CR)$ vs $1/T$ gave a straight line with a slope equal to E_a/R from which the activation energy values for both corrosion and inhibition processes were calculated. The Arrhenius plots are shown in Figure 9. The enthalpy and entropy of activation for the metal dissolution process are determined using the transition state equation 13:

$$CR = \frac{RT}{Nh} \exp\left(\frac{\Delta S^\ddagger}{R}\right) \exp\left(\frac{-\Delta H^\ddagger}{RT}\right), \quad (13)$$

where h is Planck's constant and N is Avogadro's number. A plot of $\ln(CR/T)$ vs $1/T$ gave a straight line shown in Fig. 10 with a slope = $(\Delta H^\ddagger/R)$ and an intercept = $\ln\left(\frac{RT}{Nh}\right) \exp\left(\frac{\Delta S^\ddagger}{R}\right)$. The calculated values of activation parameters are given in Table 4.

Energy of activation decreased with an increase in the inhibitor concentration due to gradual adsorption of inhibitor molecules on AA6061, this decrease being suggestive of the chemical adsorption of the inhibitor on the surface of the metal [30, 31]. A chemisorption

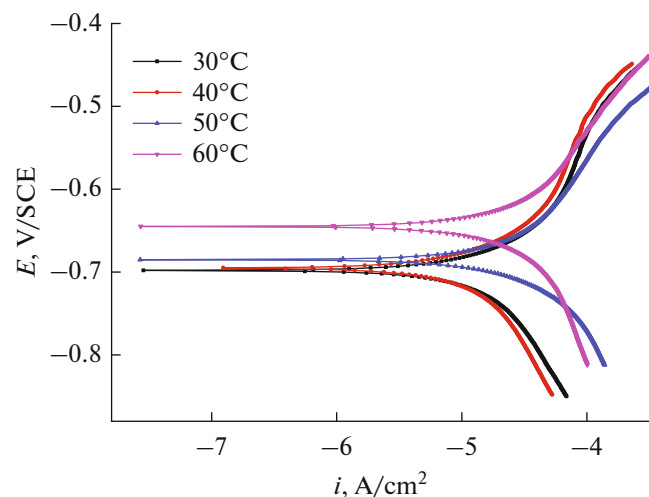
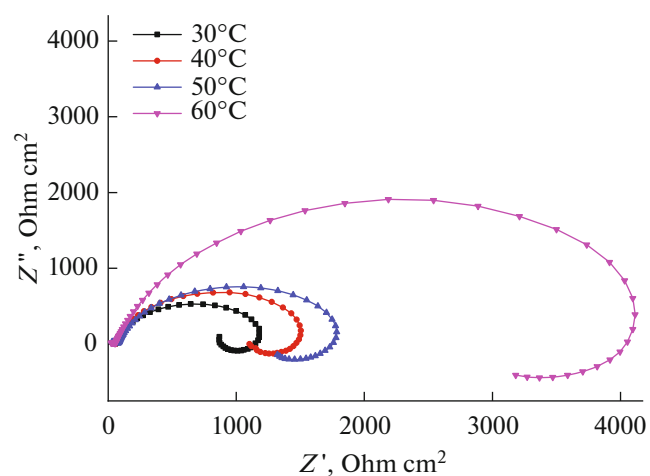
Table 3. Data obtained from EIS when AA6061 is exposed to 0.1 M HCl at various concentrations of inhibitor, at various temperatures

Temp, °C	Conc. of inhibitor, ppm	R_{ct} , $\Omega \text{ cm}^{-2}$	C_{dl} , $\mu\text{F cm}^{-2}$	%IE
30	Blank	15.70	1785.00	–
	10	61.63	134.00	74.6
	20	79.35	100.00	80.3
	30	81.21	59.16	81.0
	40	112.00	50.48	86.1
40	Blank	9.63	3761.00	–
	10	51.18	309.43	81.2
	20	56.00	285.06	85.3
	30	79.90	202.18	87.9
	40	95.50	133.02	90.0
50	Blank	5.70	12936.00	–
	10	49.70	683.81	88.5
	20	56.00	616.76	89.8
	30	70.19	398.42	91.8
	40	76.47	320.33	92.5
60	Blank	1.90	55870.00	–
	10	23.50	2642.90	91.9
	20	26.12	1166.10	92.7
	30	30.25	993.51	93.7
	40	32.40	736.57	94.1

process involves charge transfer from the inhibitor molecule to the metal surface to form a coordinate type of bond. High negative values of entropy of activation in the absence or in the presence of the inhibitor imply that the activated complex in the rate determining step is an association rather than a dissociation [32], resulting in a decrease in the randomness on going from the reactants to the activated complex [33].

Adsorption Isotherm

A clear picture of the adsorption mechanism is obtained from the adsorption isotherms such as those of Langmuir, Temkin, Frumkin, and Flory-Huggins. The degrees of the surface coverage θ obtained from PDP were fitted to the above isotherms. If the linear regression coefficient (R^2) and the slopes are close to 1, then the best fit is the Langmuir adsorption iso-

**Fig. 7.** Tafel Plots for AA6061 in 0.1 M HCl at temperatures 30–60°C.**Fig. 8.** EIS curves for AA6061 at different temperatures.

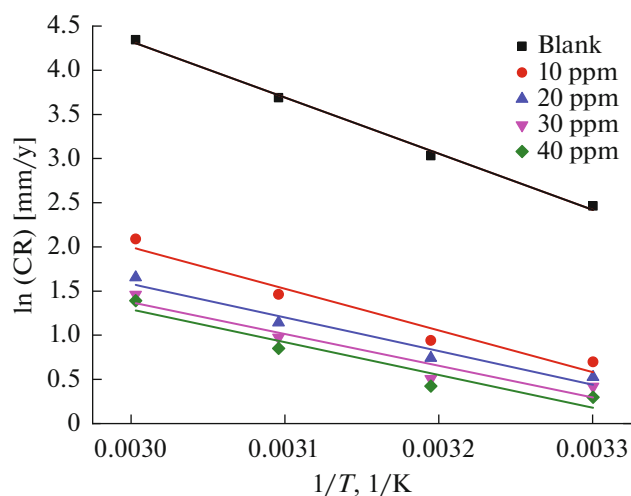


Fig. 9. Arrhenius plots for corrosion inhibition of AA6061 in 0.1 M HCl.

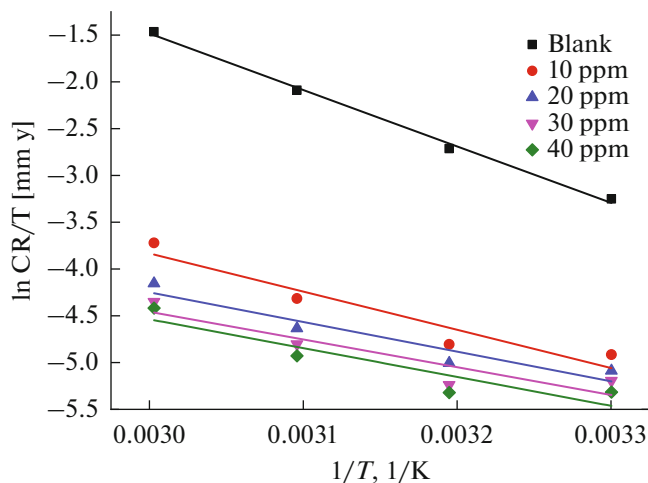


Fig. 10. Plots of $\ln CR/T$ vs. $1/T$ for corrosion inhibition of AA6061 in 0.1 M HCl.

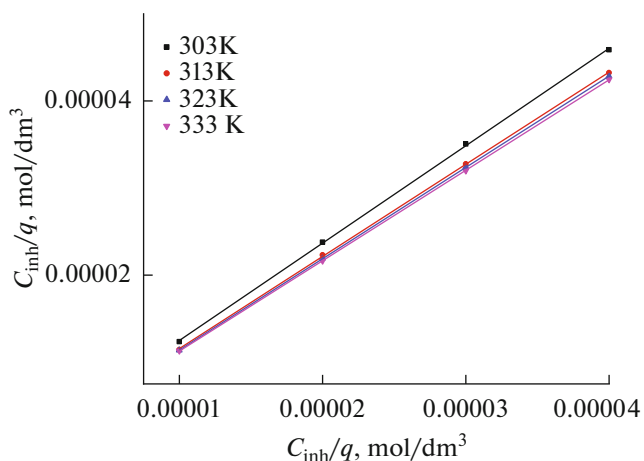


Fig. 11. Langmuir adsorption isotherm for adsorption of inhibitor on AA6061 surface at different temperatures.

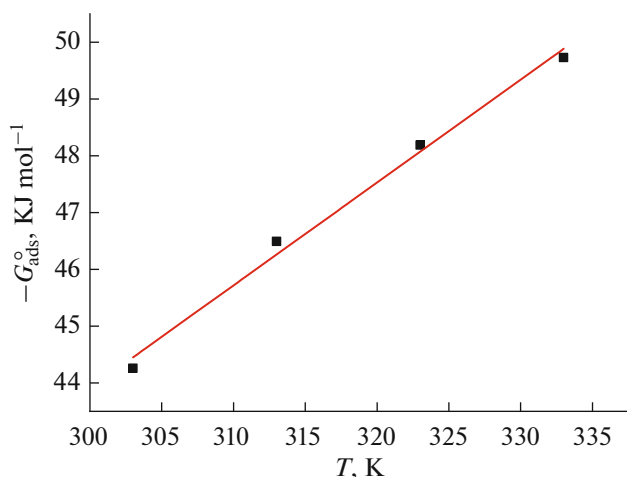


Fig. 12. Plot of ΔG_{ads}^0 vs T for adsorption of inhibitor on AA6061 in 0.1 M HCl.

therm for monolayer chemisorption as is given by Equation 14, borrowed from [34]:

$$\frac{C_{inh}}{\theta} = \frac{1}{K} + C_{inh}, \quad (14)$$

Table 4. Activation parameters for corrosion inhibition of AA6061 in 0.1 M HCl at various concentrations of inhibitor

Conc. of inhibitor, ppm	E_a , kJ mol^{-1}	ΔH^\ddagger , kJ mol^{-1}	$-\Delta S^\ddagger$, kJ mol^{-1}
Blank	52.76	50.11	86.10
10	39.16	33.95	127.50
20	31.59	26.38	153.60
30	30.81	25.61	158.38
40	29.86	24.66	160.54

where K is the equilibrium constant for the metal-inhibitor interaction, C_{inh} is the inhibitor concentration and θ is the surface coverage. The plot of C_{inh}/θ vs C_{inh} was a straight line with an intercept $1/k$ as shown in Figure 11.

Further the standard free energy change ΔG_{ads}^0 values for the adsorption were calculated using Equation 15:

$$K = \frac{1}{55.5} \exp\left(\frac{\Delta G_{ads}^0}{RT}\right), \quad (15)$$

where K is the equilibrium constant, R is the universal gas constant, T is the absolute temperature, and 55.5 is the concentration of water in solution in mol/dm^3 [35]. Figure 12 demonstrates the plot of ΔG_{ads}^0 vs T . The standard enthalpy of adsorption (ΔH_{ads}^0) and standard entropy of adsorption (ΔS_{ads}^0) were calculated from the slope and the intercept of the straight line,

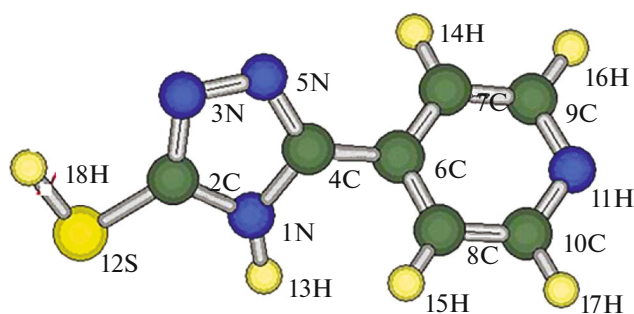


Fig. 13. 3-D presentation of PHTT molecule.

Table 5. Thermodynamic parameters for adsorption of inhibitor on AA6061 at different temperature

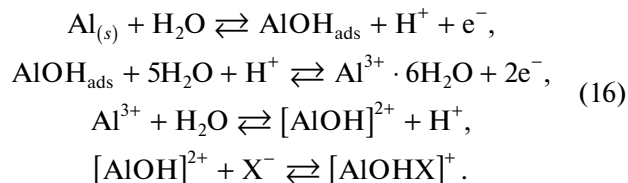
Temp °C	$-\Delta G_{\text{ads}}^{\circ}$, kJ/mol	$\Delta S_{\text{ads}}^{\circ}$, kJ/mol/K	$\Delta H_{\text{ads}}^{\circ}$, kJ/mol
30	44.26	-104.22	18.11
40	46.49		
50	48.19		
60	49.73		

respectively, and are listed in Table 5. The negative values of $\Delta G_{\text{ads}}^{\circ}$ ensured the spontaneity of the adsorption process and stability of the adsorbed layer on the alloy. Generally, if $\Delta G_{\text{ads}}^{\circ}$ are around -20 kJ mol^{-1} or lower, then it is physisorption, but if the values are more negative than -40 kJ mol^{-1} , it involves sharing of the charge or transfer of the charge from the inhibitor molecule to the metal surface to form a coordinate bond (chemisorption) [36]. In the present study, $\Delta G_{\text{ads}}^{\circ}$ values were above -40 kJ mol^{-1} indicating that adsorption of PHTT on the AA6061 surface may be completely due to chemisorption. Also, a positive value of $\Delta H_{\text{ads}}^{\circ}$ is attributable to chemisorption. Negative $\Delta S_{\text{ads}}^{\circ}$ values indicate that a decrease in disordering takes place on going from reactant to adsorbed species.

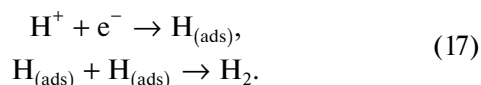
Inhibition Mechanism

Al reacts with O forming an aluminium oxide which protects the metal from corrosion in a neutral medium. But when Al is exposed to an acidic medium, the following reactions take place:

Anodic reaction:



Cathodic reaction:



So the metal undergoes dissolution at the anode and, at the cathode, hydrogen liberation takes place. An effective inhibitor alters the rate of metal dissolution and thereby controls the corrosion process. In the present study, the inhibitive action of PHTT can be explained on the base of available lone pairs of electrons on N and S atoms and π electron interaction of the benzene nucleus with unshared p electrons of Al atoms. Lone pairs of electrons on N and S is readily available for sharing with metal atoms to form a native covalent bond. Hence, the adsorbed inhibitor will cover and protect the metal surface from corrosion [37]. Three dimensional presentation of the inhibitor molecule is shown in Fig. 13, which indicates an active site for the metal inhibitor interaction. A dark yellow coloured atom is S and blue coloured atoms are N atoms which are electron rich centres.

As far as the inhibition process is concerned, it is generally assumed that adsorption of an inhibitor at the metal/solution interface is the first step in the action mechanism of inhibitors in aggressive acidic media. The adsorption may be the result of one or more of three types of interactions, namely; electrostatic attraction between charged molecules and charged metal, coordination of the unshared pairs of electron on the molecule to the metal atom, and involvement of π electrons of the inhibitor molecule in the coordination process [38]. Chemical adsorption is

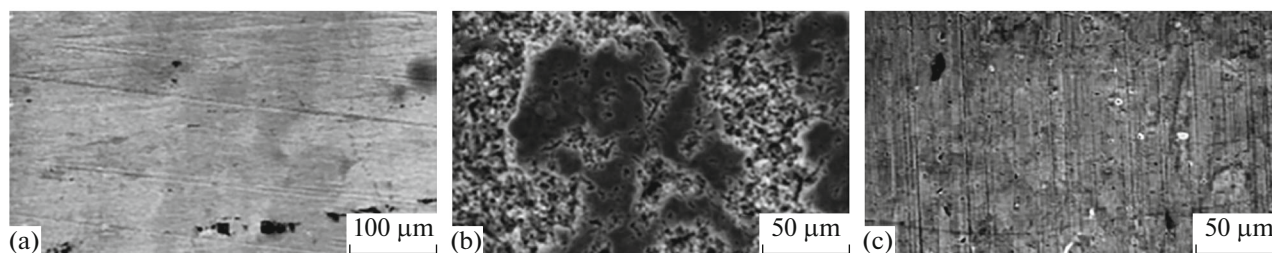


Fig. 14. SEM images of AA6061: (a) freshly polished; (b) exposed to 0.1 M HCl; (c) exposed to 0.1 M HCl containing 40 ppm of PHTT for 2h.

suggested because the metal surface is protected due to the formation of a co-ordinate bond between the metal and the inhibitor molecule. Formation of a protective film on the metal surface is also confirmed by scanning electron microscopy (SEM) image in Fig. 14.

Scanning Electron Microscopy

SEM investigations were carried out to distinguish between the surface morphology of AA6061 after immersing in 0.1 M HCl in the presence or absence of the inhibitor for about 2 h. Figure 14a shows the freshly polished alloy surface; scratches were seen possibly due to abrasion with emery sheets. Figure 14b depicts the formation of pits and accumulation of corrosion products due to an acid attack. Figure 14c confirms that inhibitor protects the alloy against corrosion through the formation of a protective film when kept in 40 ppm of PHTT for 2 hours in acidic medium.

CONCLUSIONS

PHTT was found to be an effective corrosion inhibitor for AA6061 in 0.1 M HCl, which is the base for the following conclusions:

- (1) PDP studies showed that an increasing concentration of the inhibitor effectively reduces the corrosion rate of AA6061.
- (2) The inhibition efficiency increased at higher concentrations of the studied inhibitor and temperature.
- (3) The adsorption mode was found to obey the Langmuir isotherm.
- (4) The studied inhibitor acts as potential compound by controlling metal dissolution and hydrogen liberation, there by acting as mixed type of inhibitor.
- (5) The values of the activation energy and thermodynamic parameters strongly favour chemisorption process.
- (6) Formation of a protective film on the metal surface was revealed via SEM.

REFERENCES

1. Oguzie, E.E., *Corros. Sci.*, 2007, vol. 49, pp. 1527–1539.
2. Roberts, J.D. and Caserio, M.C., *Basic Principles of Organic Chemistry*, Menlo Park, CA: W.A Benjamin, 1964.
3. Stansbury, E.E. and Buchanan, R.A., *Fundamentals of Electrochemical Corrosion*, Materials Park: ASM Int., 2000.
4. Sukiman, N.L., Zhou, X., Birbilis, N., Hughes, A.E., et al., *Durability and Corrosion of Aluminum and its Alloys: Overview, Property Space, Techniques and Developments*, Rijeka: InTech Open, 2011. pp. 49–97.
5. Ghali, E., *Corrosion Resistance of Aluminum and Magnesium Alloys: Understanding, Performance, and Testing, Wiley Series in Corrosion*, Revie, R.W., Ed., Hoboken, NJ: Wiley, 2010, pp. 3–48.
6. Sanaulla Pathapalya Fakrudeen, Ananda Murthy, H.C., and Bheema Raju, V., *J. Chil. Chem. Soc.*, 2012, vol. 57, pp. 1364–1371.
7. *Cleaning and Descaling Stainless Steel*, A Designers' Handbook Series no. 9001, Washington, DC: Am. Iron Steel Inst., 1982, pp. 2–36.
8. Ezeoke, A.U., Obi-Egbedi, N.O., Adeosun, C.B. and Adeyemi, O.G., *Int. J. Electrochem. Sci.*, 2012, vol. 7, no. 1, pp. 5339–5355.
9. El-Etre, A.Y., *Mater. Chem. Phys.*, 2008, vol. 108, nos. 2–3, pp. 278–282.
10. Ahamad, I. and Quraishi, M.A., *Corros. Sci.*, 2009, vol. 51, pp. 2006–2013.
11. Zhang, Q.B. and Hua, Y.X., *Electrochim. Acta*, 2009, vol. 54, pp. 1881–1887.
12. Quraishi, M.A., Sardar, N., and Ali, H., *Corros. Sci.*, 2002, vol. 58, pp. 317–321.
13. Prakashaiah, B.G. and Nityananda Shetty, A., *Surf. Eng. Appl. Electrochem.*, 2018, vol. 54, no. 3, pp. 286–296.
14. Harvey, T.G., Hardin, S.G., Hughes, A.E. and Munster, T.H., *Corros. Sci.*, 2011, vol. 53, pp. 2184–2190.
15. Fontana, M.G., *Corrosion Engineering*, New York: McGraw-Hill, 1986.
16. Charitha, B.P. and Padmalatha Rao, *India J. Mater. Environ. Sci.*, 2017, vol. 8, pp. 78–89.
17. Ferreira, E.S., Giancomelli, C., Giacomelli, F.C., and Spinelli, A., *Mater. Chem. Phys.*, 2004, vol. 83, pp. 129–134.
18. Li, W.H., He, Q., Pei, C.L., and Hou, B.R., *Electrochim. Acta*, 2007, vol. 52, pp. 6386–6394.
19. Li, W.H., He, Q., Pei, C.L. and Hou, B.R., *J. Appl. Electrochem.*, 2008, vol. 38, pp. 289–295.
20. Njoku, V.O., Oguzie, E.E., Obi, C., and Ayuk, A.A., *Adv. Chem.*, 2014, vol. 10, pp. 1155–1125.
21. Rosliza, R., Senin, H.B., and Wan Nik, W.B., *Colloids Surf., A*, 2008, vol. 312, pp. 185–189.
22. Lebrini, M., Robert, F., Blandinieres, P.A. and Roos, C., *Int. J. Electrochem. Sci.*, 2011, vol. 6, pp. 2443–2460.
23. Prasanna, B.M. and Praveen, B.M., *Anti-Corros. Methods Mater.*, 2016, vol. 63, pp. 47–55.
24. Pinto, G.M., Nayak, J., and Nityananda Shetty, A., *Mater. Chem. Phys.*, 2011, vol. 125, pp. 628–640.
25. Migahed, M.A., *Mater. Chem. Phys.*, 2005, vol. 93, pp. 48–53.
26. Singh, A.K. and Quraishi, M., *Corros. Sci.*, 2010, vol. 52, pp. 152–160.
27. *Impedance Spectroscopy, Theory, Experiment, and Applications*, Barsoukov, E. and Ross Macdonald, J., Eds., New York: Wiley, 2005, 2nd ed.
28. Machnikova, E., Kenton, W.H., et al., *Electrochim. Acta*, 2008, vol. 53, pp. 6024–6032.
29. Zucchi, F., Grassi, V., Frignani, A., Monticelli, C., et al., *J. Appl. Electrochem.*, 2005, vol. 36, pp. 195–204.
30. Osman, M.M., El-Ghazawy, R.A., and Al-Sabagh, A.M., *Mater. Chem. Phys.*, 2003, vol. 80, pp. 55–62.

31. Ashassi-Sorkhabi, H., Shaabani, B., and Seifzadeh, D., *Appl. Surf. Sci.*, 2005, vol. 239, pp. 154–164.
32. Hamdy, A. and El-Gendy, N.S., *Egypt. J. Petrol.*, 2013, vol. 22, pp. 17–25.
33. Soltani, N., Behpour, M., Ghoreishi, S.M., and Naeimi, H., *Corros. Sci.*, 2010, vol. 52, pp. 1351–1361.
34. Paul, S. and Kar, B., *Corrosion*, 2012, art. ID 641386.
35. Sanaulla Pathapalya Fakrudeen, Ananda Murthyh, and Bheema Raju, V., *J. Chil. Chem. Soc.*, 2012, vol. 57, pp. 1364–1370.
36. Martinez, S. and Stern, I., *Appl. Surf. Sci.*, 2002, vol. 199, pp. 83–86.
37. Rajenran, S., *J. Electrochem. Soc.*, 2005, vol. 54, no. 2, pp. 61–71.
38. Schweinsberg, D., George, G., Nanayakkara, A., and Steiner, D., *Corros. Sci.*, 1988, vol. 28, pp. 33–42.